Research Article | Vol. 28, No. 2 / 20 January 2020 / Optics Express 2547

Optics EXPRESS

Multi-resonance and ultra-wideband terahertz metasurface absorber based on micro-template-assisted self-assembly method

DAQUAN YANG,[1,2,4] CHAO ZHANG,[1] XIACAO JU,[1] YUEFENG JI,[1,5] AND CHUWEN LAN[1,3,6]

[1] *State Key Laboratory of Information Photonics and Optical Communications, and School of information and communication Engineering, Beijing University of Posts and Telecommunications, Beijing, China*
[2] *State Key Laboratory of Terahertz and Millimeter Waves, and Department of Electronic Engineering, City University of Hong Kong, Hong Kong, China*
[3] *State Key Laboratory of Millimeter Waves, Southeast University, Nanjing, China*
[4] *ydq@bupt.edu.cn*
[5] *jyf@bupt.edu.cn*
[6] *lanchuwen@126.com*

Abstract: As a promising platform for multi-functional terahertz devices, metasurface absorbers have received widespread attention in recent years. However, due to the existence of manufacturing difficulties, high cost, fragility, single or narrow absorption and other disadvantages, their application ranges are severely limited. Therefore, to effectively solve these problems, we have designed a flexible and high-precision terahertz metasurface absorber based on the micro-template assisted self-assembly method. Free from high cost, complicated process and time-consumption, the sandwich structure terahertz metasurface absorber consisting of a ceramic microspheres layer, a dielectric spacer layer, and a metal copper film is fabricated economically. On the one hand, through assembling the microspheres on the dielectric spacer in a periodic pattern arrangement, multiple resonances can be observed with a maximum absorption rate of up to 92.5% at 0.745 THz and are insensitive to the polarization of incident light. On the other hand, by attaching the microspheres to the dielectric layer in a compact configuration, 90% absorption bandwidth beyond 1.2 THz can be observed with a central frequency of 1.8 THz. The theoretical model of multiple reflection and interference is employed to explain these absorption characteristics. Considering the flexible design and high-throughput manufacturing processes, this work provides a promising platform for the development of high-efficiency and multi-functional terahertz devices.

1. Introduction

Terahertz (THz) wave, a wave of frequency ranges from 0.1 THz to 10 THz, has attracted much academic attention in recent decades, owing to its unique application in biological medicine, detection, security imaging, high-speed wireless communication, etc. [1–6]. However, the lack of high-performance functional devices has made the rapid developments of THz technology very hampered. Fortunately, due to the singular electromagnetic response to THz radiation, metasurface provides a promising platform for the THz multi-functional devices [7–12]. One of the most meaningful branches of these devices is the metasurface absorber, which can achieve near-unity absorption of THz radiation by matching the effective impedance of the free space to minimize reflectivity [13]. The first design of the metasurface perfect absorber composed of a sandwich structure was proposed by Landy et al, in 2008, which obtained an absorption above 88% at the resonance frequency of 11.5 GHz [14]. Subsequently, with the gradual maturation of theoretical analysis and manufacturing processes, various designs of THz

#381927 https://doi.org/10.1364/OE.381927
Journal © 2020 Received 31 Oct 2019; revised 8 Jan 2020; accepted 8 Jan 2020; published 17 Jan 2020

metasurface absorbers were proposed and confirmed. Nowadays, as an important part of the THz equipment, metasurface perfect absorbers have been widely used in sensing, modulation, thermal emission, communication, and so on [15–19].

Metasurface perfect absorbers are typically designed as a three-layer structure, a periodic pattern layer, a dielectric spacer layer and a metal ground plane [20]. By optimizing the geometry of the structure and selecting the appropriate materials, metasurface absorbers can exhibit unique absorption characteristics, such as multiple or broad resonance, wide-angle, polarization insensitivity and narrow discrete distance of resonance frequencies [21–23]. Among those, the multi-resonance absorber is one of the most important portions. Multi-resonance absorber can be designed with three methods [24]: 1) to design multiple absorber units with different resonant frequencies in the same plane, known as the coplanar construction method; 2) to stack different sizes of absorber elements in a vertical space, termed the vertical stacking method; 3) to combine the two methods mentioned before. Interestingly, all of these approaches can also be used to realize broadband absorption by adjusting the dimension of these elements appropriately, which is another significant characteristic of the THz metasurface absorbers [25,26]. For example, B.-X. Wang proposed a four-band and polarization-insensitive terahertz absorber consisting of four square metal rings with different sizes on the same plane [27]. W. Pan demonstrated a broadband terahertz metamaterial absorber based on the longitudinal coupling of the nest structure with different geometric parameters in a vertical space [28]. However, because too many absorber elements of different sizes are required in the unit cell structure, all of these methods to achieve multi-resonance or broadband absorbers have the same limitations. Firstly, the existing manufacturing methods have difficulty in achieving a good balance between high precision, time-consuming and cost. Secondly, it is hard to resolve the coordination between the absorption band and the absorption area. Thirdly, the thickness of these metasurfaces cannot be well controlled, which increases the difficulty of device integration. As a result, most metasurface perfect absorbers have only achieved dual-resonance absorption, narrow band performance or implemented theoretically, which limits the application range of absorber in THz high efficient devices. Therefore, the experimental realization of multi-resonance and ultra-broadband absorber with low cost and high-precision is of great significance.

In order to achieve this target, in this work, flexible and high precision terahertz metasurface absorbers based on the micro-template assisted self-assembly (MTAS) method are proposed [29]. Free from cost, complex process and time-consuming, the sandwich structure terahertz metasurface absorber consisting of Zirconia (ZrO_2) microspheres and a metal ground plane separated by a polyimide spacer is fabricated economically. On the one hand, by arranging the microspheres into a periodic pattern arrangement, the maximum multi-band absorption can up to 92.5% at a frequency of 0.745 THz. On the other hand, through assembling the microspheres on the polyimide spacer in a compact configuration, 90% absorption bandwidth beyond 1.2 THz with a central frequency of 1.8 THz is observed, which exhibits superior absorption property. The theoretical model of multiple reflection and interference is employed to explain these characteristics. At the same time, both of the metasurface absorbers are insensitive to the polarization of the THz wave at oblique incidence. Considering the flexible design and high throughput manufacturing processes, this work provides a promising platform for the development of high-efficiency and multi-functional terahertz devices.

2. Design and fabrication

In order to realize the flexibility, high-precision and simple manufacturing of the THz metasurface absorber, the micro-template-assisted self-assembly (MTAS) method is employed in the sample manufacturing process. In Fig. 1(a) is the fundamental process of the MTAS method. First, a metal template with periodic hole arrays as shown in Figs. 1(b)–1(c) is fabricated and attached to a target dielectric spacer. Then, the prepared uniform microsphere particles are transferred to the template and a soft brush is used to push the microspheres from left to right repeatedly. Since the diameter of the array of holes is slightly larger than the diameter of these particles, the microspheres are pushed into the holes and arranged periodically. Please note that a thin layer of glue is used between the template and the dielectric spacer to fix these microspheres. Thereafter, the template is removed and well-arranged microspheres are obtained on the dielectric spacer, as shown in Fig. 1(d). Finally, a copper film is deposited on the other side of the dielectric spacer through magnetron sputtering. The flexibility and high-precision metasurface absorber is obtained in Fig. 1(e). As expected, the microscopic image of the sample is depicted in Fig. 1(f), and microspheres of the same size are periodically arranged on the dielectric spacer.

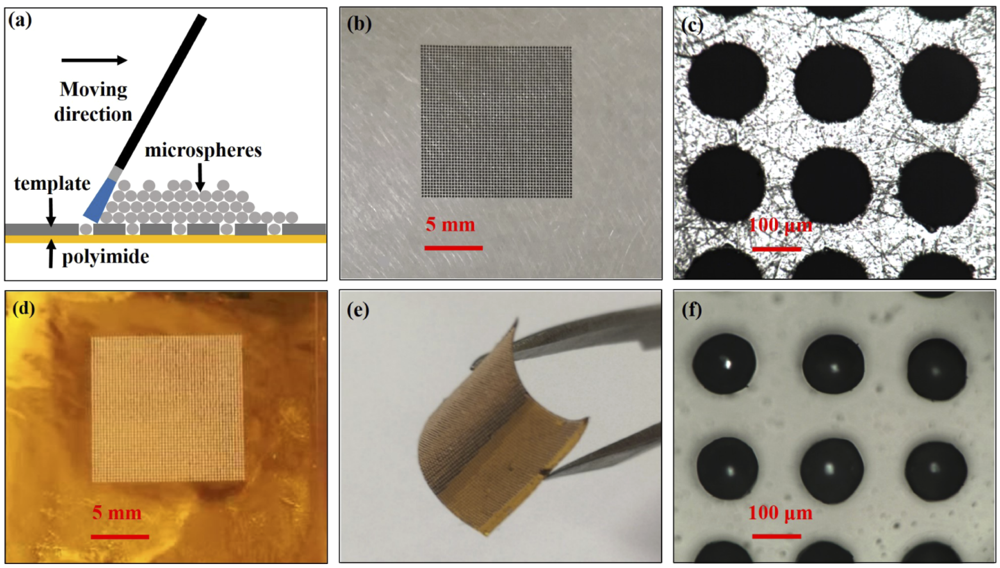

Fig. 1. (a) Illustrations of the micro-template-assisted self-assembly method. (b) Physical image and (c) microscopic image of the metal template. (d) Physical image of the microspheres periodically arranged on the dielectric spacer. (e) Physical and (f) microscopic images of the fabricated sample.

For the preparation of the template, first, a stainless steel membrane with uniform thickness is placed on the workbench. The appropriate AutoCAD file is then written to and input to the controller, which synchronizes the table with the laser to etch the membrane. The stainless steel membrane is written point-by-point using a solid-state laser (Enpon-Nano-H532, a nanosecond laser) that is operated at 532 nm with a 7 W output energy and a 10 ns pulse duration. Before etching the next hole, the laser must be turned off to avoid damaging the area between two adjacent holes. Finally, the template with a periodic hole pattern is obtained. During fabricating the sample, first, we transferred the uniform microspheres onto the polyimide layer, then deposited a copper film on the polyimide spacer by radio frequency magnetron sputtering. The base pressure is 10^6 Pa to ensure a low impurity level. For the growth conditions, 55 W radio frequency power and 0.6 Pa Ar pressure are used to ensure good uniformity of the copper film. The sample is deposited for ten minutes to obtain a copper film with a thickness exceeding the skin depth of THz radiation.

In order to obtain a high-performance terahertz absorber, the structural design of the metasurface is determined through simulation and experiment. First, the permittivity and loss tangent of zirconia microspheres and polyimide are obtained from Refs. [30-31]. Then, to achieve the multi-resonant absorption of the metasurface, the parameter sweep of the CST Microwave Studio is employed to determine the structural design. Next, the sample of the absorber is fabricated based on the simulated results, and the permittivity and loss tangent of the zirconia and polyimide are determined experimentally. Finally, the structural parameters of the metasurface absorber are optimized by using the experimental permittivity and loss tangent. In the experiment, a 150-μm-thick stainless-steel membrane with periodic hole array (period = 200 μm) is selected as the template. The smooth, uniform and ZrO_2 ceramic spheres with a diameter of 130 μm are employed as microspheres. Assuming that the permittivity of ZrO_2 is 40 and the loss tangent is 0.15, respectively [30]. In the experiment, the dielectric spacer is a 50 μm thick polyimide with a low permittivity ($\epsilon = 3.6$) and a low loss tangent (loss tangent = 0.01) [31]. Considering the balance between performance and efficiency, the thickness of the copper film is set to 400 nm. Through this method, flexibility and high-precision samples are fabricated without complicated process and time-consuming.

3. Experiment and discussion

The typical schematic setup of a terahertz time-domain spectroscopy (THz-TDS) system and experimental equipment are shown in Figs. 2(a)–2(b). The major components of the THz-TDS system are a Ti: sapphire femtosecond laser, an LT-GaAs THz emitter source, a ZnTe THz detector, focusing and collimating parts for laser, mirrors, sample, a motorized delay line, a lock-in amplifier, and a signal analysis system. The usable bandwidth of the THz-TDS is from 0.1 THz to 3 THz, and the resolution is below 5 GHz to provide enough spectrum information. The detector with a scanning accuracy of less than 2 μm is used for information collection and analysis. In the experiment, considering the absorption and dispersion of the THz beams by water vapor, nitrogen gas is used to control the content of water vapor below 5%. The fabricated sample is characterized by reflection when THz radiation is focused onto the sample at oblique incidence. In order to normalize the reflection of the sample, the reference is measured by replacing the sample with a metal patch. As a result, the normalized reflection is defined as $|R_{sample(\omega)}/R_{reference(\omega)}|$, where $R_{sample(\omega)}$ and $R_{reference(\omega)}$ are the reflection of the sample and the reference, respectively. In general, the absorption is given by $A(\omega) = 1 - R(\omega) - T(\omega)$, where $R(\omega)$ and $T(\omega)$ are the reflection and transmission of the terahertz metasurface, respectively.

Figure 3(a) shows the measured absorption spectrum of the fabricated sample using a THz-TDS system. Three remarkable resonance peaks can be observed ranging from 0.3 THz to 0.8 THz, and the maximum absorption rate can reach 92.5% at 0.745 THz, which exhibits the great multi-resonance absorption characteristic of the sample. To have a deeper understanding of the multi-resonance absorption properties, CST Microwave Studio is used to verify the experiment results. Unit cell boundary conditions are employed with a frequency domain plane wave pulse at oblique incidence to match experiment settings. As plotted in Fig. 3(a), triple-band resonances are obtained with three absorption values of 66.9% at 0.384 THz, 87.1% at 0.520 THz and 99.2% at 0.745 THz, which have the same resonance frequency as the experimental measurements. As a result, good agreement can be observed between the simulation and the experimental result, confirming the high quality of the fabricated sample. However, compared with simulation result, the absorption of the measurement is slightly lower on the whole. These disagreements can be explained by the following reasons: (i) the geometric parameters of the fabricated sample may be slightly different from the design and the ZrO_2 particles are not standard spheres; (ii) the permittivity and loss tangent of these materials may have deviations in experiment and simulation; (iii) the influence of the glue used in the manufacturing process is not considered in the numerical calculation. For the measured and simulated results on the oblique incidence condition, multiple reflection and interference theory is used for qualitative analysis and interpretation of the absorption properties [32–34]. As shown in Fig. 3(b), we assume that the dielectric spacer and the pattern layer are considered as a whole, which is called as area1, and the copper film used in the experiment is considered as the ground plane. In the theoretical model, $r_{12}e^{i\theta 12}$ represents the air to air reflection coefficient at the interface; $r_{21}e^{i\theta 21}$ is the reflection coefficient from area1

Optics EXPRESS

to area1 at the interface; $t_{12}e^{i\varphi 12}$ indicates the transmission coefficient from air to area1 at the interface, and $t_{21}e^{i\varphi 21}$ is the transmission coefficient from area1 to air at the interface. According to the interference theory and the existence of the ground plane, the overall reflection of the model can be expressed as:

$$r = r_{12}e^{j\theta_{12}} + \frac{t_{12}t_{21}e^{j(\varphi_{12}+\varphi_{21}-2\beta-\pi)}}{1 - r_{21}e^{j(\theta_{21}-2\beta-\pi)}} \tag{1}$$

where $\beta = kd$ is the propagation phase and k is the wavenumber in area1, d is the propagation distance of the transmitting wave from interface to ground plane. Therefore, the absorption can be calculated through $A(\omega) = 1 - R(\omega) - T(\omega) = 1 - |r|^2$ since the transmission $T(\omega) = 0$ due to the existence of ground plane. The perfect absorption of the metasurface can be obtained with the satisfaction of the interference theory. As shown in Fig. 3(a), the calculated absorption spectrum (in green line) is in general agreement with results from both experiment (in black line) and simulation (in red line). The differences can be explained by the following reasons: (i) the difference between dielectric microspheres used in this paper and the metal resonators in Refs. [32–34]; (ii) the deviation results from the process of considering the dielectric spacer and the pattern layer as a whole. From the analysis results we can speculate that the absorptivity of metasurface absorber is mainly related with the scattering characteristic of the resonator. On the contrary, the main contribution of the ground plane is to reflect the incident THz waves. To validate our theoretical analysis, the metasurface without copper film is also simulated as indicated in Fig. 3(a). Because the condition of interference theory is destroyed, absorption of the metasurface without copper film is obviously below than that with the copper film, which is consistent with our analysis.

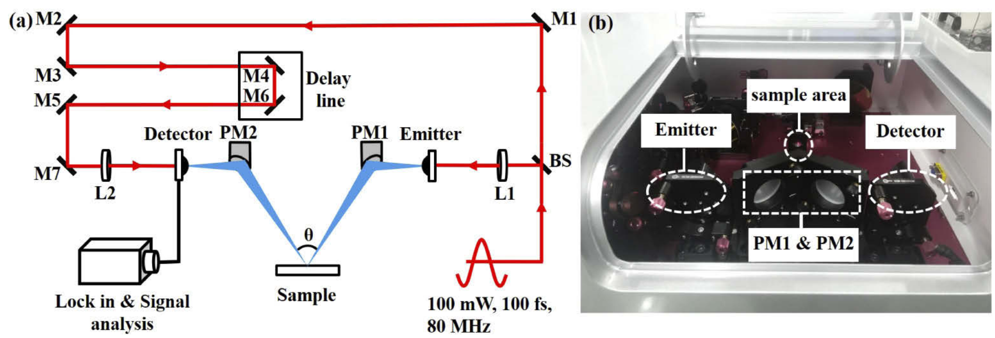

Fig. 2. (a) Schematic of the terahertz time-domain spectroscopy system used in experiments, where M1-M7 represent optical mirrors, BS represents the beam splitter and PM represents the parabolic mirror. The angle θ is equal to 90°. (b) Measured equipment for the terahertz metasurface absorbers.

Considering the influence of the geometric parameters on the metasurface characteristics, the absorption associated with the thickness of the dielectric spacer can be simulated by directly varying the thickness from 40 μm to 60 μm. As demonstrated in Fig. 4(a), the absorption at 0.384 THz increases obviously with the decreases of the thickness of the dielectric spacer. This means that for the first resonance mode, the unity-absorption can always be achieved with an optimized spacer thickness. Since the second and third resonance modes are mainly dependent on the sizes of the microspheres, their absorption spectra change relatively little as the thickness of the dielectric spacer decreases. Therefore, as shown in Fig. 4(b), the relationship between absorption resonance modes and microspheres has also been studied. As obtained from the spectra, the unit-cell structure of the metasurface absorber with different microsphere diameters or periods are simulated when other geometric parameters are fixed. Originally, the microspheres

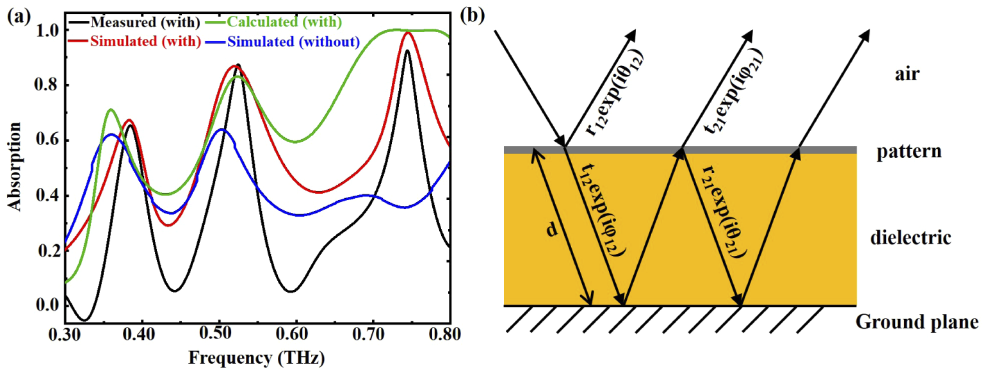

Fig. 3. (a) Measured, simulated and calculated absorption spectrum of the metasurface absorber, and the contrast simulated absorption spectrum of a metasurface without the copper film. (b) The theoretical model of multiple reflections and interferences at oblique incidence, where the microspheres are represented by the gray line at the air-dielectric interface.

are arranged in a square array with diameter d = 65 μm and period P = 200 μm. when P = 200 μm and P = 210 μm with d = 65 μm are compared in Fig. 4(b), the first two low-frequency resonance modes hardly change while the third resonance shifts to a lower frequency. While the absorption of the resonance at 0.745 THz remains above 99% with the variation of period, it shows the high stability of the device. Besides, when the diameter of microsphere increases from 65 μm to 70 μm with the period remains 200 μm, the first and second resonances show redshifts 0.017 THz and 0.021 THz, respectively. In the contrary, a slight blue shift 0.013 THz of the third absorption peak is observed in Fig. 4(b). This is an interesting and worthwhile phenomenon, which means that we can control the three absorption resonances appear at any frequency by just changing the diameter and period of the structure unit-cell. We believe that more perfect absorption characteristics can be observed by optimizing the metasurface geometric parameters. At the same time, it should be noted that although the resonant frequency of the absorber cannot be directly adjusted by external stimulation, however, it can be manufactured in large quantities to meet different application scenarios combined with the high-throughput and low-cost manufacturing process.

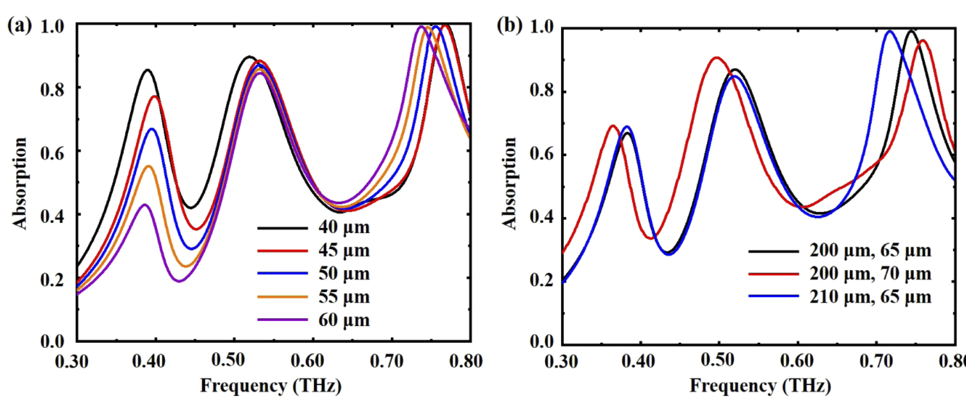

Fig. 4. (a) Simulated absorption spectrum of the metasurface with different dielectric spacer thicknesses. (b) Simulated absorption spectrum of the microspheres with different sizes or periods.

Optics EXPRESS

Besides, polarization insensitivity is also of considerable merit for terahertz metasurface absorbers in practical applications. Thus, the effect of the polarization angle on the absorption performance of metasurface is also considered. Since the proposed structure has a high degree of the fourfold rotational symmetry, it can be inferred that the absorber is insensitive to the polarization of the incident electromagnetic wave. Figure 5(a) gives the measured absorption of the sample by adjusting the polarization angle from 0° to 90°. With the increase of polarization angle, the amplitude and resonance frequency are almost unchanged, which exhibits excellent stability for the incident THz waves. At the same time, we also study the influence of incident angle on the performance of the absorber. The simulated absorption spectrum with the incident angle increasing from 35° to 65° is shown in Fig. 5(b). In the case of TM polarization, the absorption peak at 0.745 THz is slightly redshifted with the angle of incidence, while the absorption peaks at 0.384 THz and 0.520 THz are insensitive to incident angle. The insensitivity of the polarization angle and wide incident angle allows the absorber to be used in numerous applications.

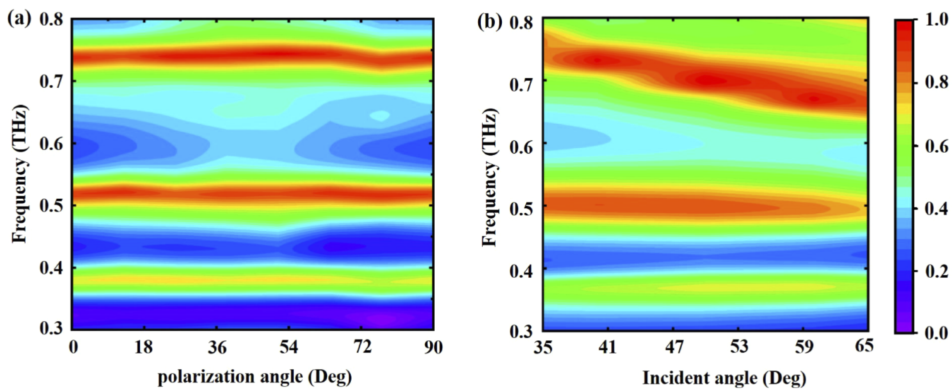

Fig. 5. (a) The measured absorption spectrum at different polarization angles of the fabricated sample. (b) The simulated absorption spectrum of the sample with different incident angles.

It is well known that in the development of terahertz metamaterials, a given unit cell is rarely used in two different applications in different frequency bands without a significant modification of the unit cell geometry. Most of these metasurfaces can only present a single function, such as multi-band absorption, broadband reflection, and frequency selective transmission. Although a variety of active or tunable materials are combined with these metasurfaces to alter their operating frequency or function, the operating modes of these devices can only be changed within a narrow frequency range. The main reason for this phenomenon is that the response of the metasurfaces to THz radiation depends mainly on their unit cell structure, and it is difficult to achieve different responses. Surprisingly, different from most metasurfaces with chemical deposition or laser etching in the fabrication of resonant unit cells, the absorbers we proposed here are great structural flexibility. As a result, during the manufacturing and testing process of the samples, we find the ultra-broadband absorption occurs in a different frequency band compared with the absorber discussed in Fig. 3(a). As demonstrated in Fig. 6(a), a non-periodic metasurface is obtained when we place the ZrO_2 microspheres on the polyimide layer without the metal template. Two types of sample are fabricated with the microspheres of different diameters d = 60 μm and d = 65 μm. As plotted in Fig. 6(b), ultra-broadband absorption has been studied in both of the measured and simulated spectra in the frequency range from 1.0 THz to 2.5 THz. It can be seen from the spectrum that 90% absorption bandwidth beyond 1.2 THz with a central frequency of 1.8 THz. The difference between the measured and simulated absorption can be attributed to the

Optics EXPRESS

existence of water vapor and glue. We consider that the wideband absorption of the metasurface is attributed to the coupling effects between the microspheres. As shown in Fig. 6(b), for the metasurface absorbers with different size microspheres, similar ultra-wideband absorption can be observed. It means that the absorption is resulted from coupling effects rather than the resonance of unit cells. This phenomenon also represents that we can realize ultra-broadband absorption without considering the influence of the diameter of microspheres. Combining advantages of free from metal membrane in the fabrication, non-periodic metasurface absorbers are more suitable for broad absorption. Finally, due to the non-periodic arrangement of the microspheres in the samples, it is no longer to consider the influence of the polarization angle on the absorber. These results show that our design can realize multi-resonance and ultra-broadband absorption without a significant modification of the unit cell structure. It provides a promising platform for the multi-functional terahertz metasurfaces.

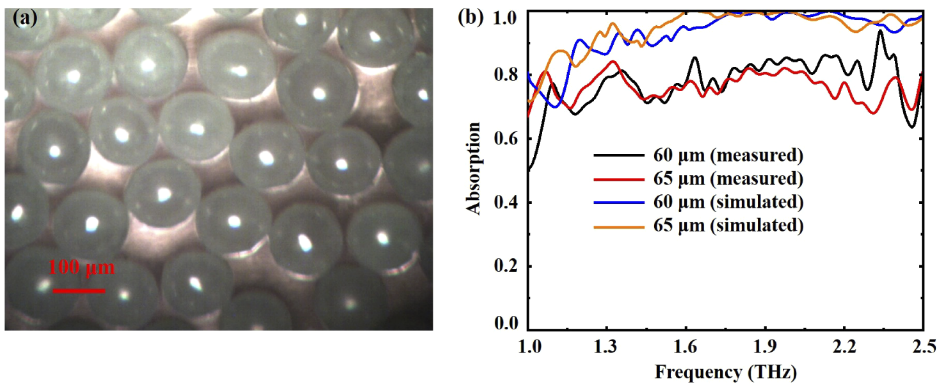

Fig. 6. (a) Microscope image of a fabricated sample from the unit cell arranged in a non-periodic pattern. (b) Measured and simulated absorption spectra of the microspheres with different diameters.

4. Conclusion

In summary, we introduce a generic design for multi-resonance and ultra-broadband metasurface absorbers based on the micro-template-assisted self-assembly method. Through assembling the microsphere resonators into a designed pattern, multi-resonances at the goal frequencies can be realized. A triple-band absorber with the maximum absorption up to 92.5% is obtained. Meanwhile, with the freedom for manipulating the microsphere resonators into any non-periodic arrangement, 90% absorption bandwidth beyond 1.2 THz with a central frequency of 1.8 THz is observed. Free from cost, complex process and time-consuming, our designs provide a versatile and powerful platform for terahertz metamaterials, which should find a wide variety of applications in multi-functional and high-efficiency terahertz devices.

Funding

National Natural Science Foundation of China (11974058, 61905021); Fundamental Research Funds for the Central Universities (2018XKJC05); State Key Laboratory of Information Photonics and Optical Communications (IPOC2019ZT03); State Key Laboratory of Millimeter Waves (K202008); Shenzhen Technical Project (JCYJ20180305164708625).

Acknowledgments

The authors thank Prof. Limei Qi from Beijing University of Posts and Telecommunications, Prof. Yongzhi Cheng from Wuhan University of Science and Technology, and Dr. Yunyun Ji from Prof. Shengjiang Chang group of Nankai University for the theoretical discussion.

Disclosures

The authors declare no conflicts of interest.

References

1. Q. Sun, Y. He, K. Liu, S. Fan, E. P. J. Parrott, and E. Pickwell-MacPherson, "Recent advances in terahertz technology for biomedical applications," Quant. Imaging Med. Surg **7**(3), 345–355 (2017).
2. K. Gallo and G. Assanto, "All-optical diode based on second-harmonic generation in an asymmetric waveguide," J. Opt. Soc. Am. B **16**(2), 267–269 (1999).
3. D. A. Bandurin, D. Svintsov, I. Gayduchenko, S. G. Xu, A. Principi, M. Moskotin, I. Tretyakov, D. Yagodkin, S. Zhukov, T. Taniguchi, K. Watanabe, I. V. Grigorieva, M. Polini, G. N. Goltsman, A. K. Geim, and G. Fedorov, "Resonant terahertz detection using graphene plasmons," Nat. Commun. **9**(1), 5392 (2018).
4. S. Gui, J. Li, and Y. Pi, "Security Imaging for Multi-Target Screening Based on Adaptive Scene Segmentation With Terahertz Radar," IEEE Sens. J. **19**(7), 2675–2684 (2019).
5. X. Yang, Y. Pi, T. Liu, and H. Wang, "Three-Dimensional Imaging of Space Debris with Space-Based Terahertz Radar," IEEE Sens. J. **18**(3), 1063–1072 (2018).
6. Q. Xia and J. M. Jornet, "Expedited Neighbor Discovery in Directional Terahertz Communication Networks Enhanced by Antenna Side-lobe Information," IEEE Trans. Veh. Technol. **68**(8), 7804–7814 (2019).
7. L. Chen, S.-W. Qu, B.-J. Chen, X. Bai, K. B. Ng, and C. H. Chan, "Terahertz Metasurfaces for Absorber or Reflectarray Applications," IEEE Trans. Antennas Propag. **65**(1), 234–241 (2017).
8. G.-B. Wu, Y.-S. Zeng, K. F. Chan, S.-W. Qu, and C. H. Chan, "3-D Printed Circularly Polarized Modified Fresnel Lens Operating at Terahertz Frequencies," IEEE Trans. Antennas Propag. **67**(7), 4429–4437 (2019).
9. B. Li, Y.-S. Zeng, B.-J. Chen, and C. H. Chan, "Terahertz Frequency Selective Surface with Polarization Selection and Conversion Characteristics," IEEE Trans. THz Sci. Technol. **9**(5), 510–519 (2019).
10. S. Tan, F. Yan, N. Xu, J. Zheng, W. Wang, and W. Zhang, "Broadband terahertz metamaterial absorber with two interlaced fishnet layers," AIP Adv. **8**(2), 025020 (2018).
11. W. Wang, F. Yan, S. Tan, H. Zhou, and Y. Hou, "Ultrasensitive terahertz metamaterial sensor based on vertical split ring resonators," Photonics Res. **5**(6), 571–577 (2017).
12. H. Cai, S. Chen, C. Zou, Q. Huang, Y. Liu, X. Hu, Z. Fu, Y. Zhao, H. He, and Y. Lu, "Multifunctional Hybrid Metasurfaces for Dynamic Tuning of Terahertz Waves," Adv. Opt. Mater. **6**(14), 1800257 (2018).
13. G. Duan, J. Schalch, X. Zhao, J. Zhang, R. D. Averitt, and X. Zhang, "Analysis of the thickness dependence of metamaterial absorbers at terahertz frequencies," Opt. Express **26**(3), 2242–2251 (2018).
14. N. I. Landy, S. Sajuyigbe, J. J. Mock, D. R. Smith, and W. J. Padilla, "Perfect metamaterial absorber," Phys. Rev. Lett. **100**(20), 207402 (2008).
15. X. Zhao, Y. Wang, J. Schalch, G. Duan, K. Cremin, J. Zhang, C. Chen, R. D. Averitt, and Z. Zhang, "Optically Modulated Ultra-Broadband All Silicon Metamaterial Terahertz Absorbers," ACS Photonics **6**(4), 830–837 (2019).
16. Q. Xie, G. Dong, B.-X. Wang, and W.-Q. Huang, "Design of Quad-Band Terahertz Metamaterial Absorber Using a Perforated Rectangular Resonator for Sensing Applications," *Nanoscale Res. Lett.*, 13(137) (2018).
17. K. Fan, J. Y. Suen, X. Liu, and W. J. Padilla, "All-dielectric metasurface absorbers for uncooled terahertz imaging," Optica **4**(6), 601–604 (2017).
18. L. Cong, S. Tan, R. Yahiaoui, F. Yan, W. Zhang, and R. Singh, "Experimental demonstration of ultrasensitive sensing with terahertz metamaterial absorbers: A comparison with the metasurfaces," Appl. Phys. Lett. **106**(3), 031107 (2015).
19. H. R. Seren, G. R. Keiser, L. Cao, J. Zhang, A. C. Strikwerda, K. Fan, G. D. Metcalfe, M. Wraback, X. Zhang, and R. D. Averitt, "Optically Modulated Multiband Terahertz Perfect Absorber," Adv. Opt. Mater. **2**(12), 1221–1226 (2014).
20. J. Schalch, G. Duan, X. Zhao, X. Zhang, and R. D. Averitt, "Terahertz metamaterial perfect absorber with continuously tunable air spacer layer," Appl. Phys. Lett. **113**(6), 061113 (2018).
21. M. L. Huang, Y. Z. Cheng, Z. Z. Cheng, H. R. Chen, X. S. Mao, and R. Z. Gong, "Design of a Broadband Tunable Terahertz Metamaterial Absorber Based on Complementary Structural Graphene," Materials **11**(4), 540 (2018).
22. B.-X. Wang, C. Tang, Q. Niu, Y. He, and T. Chen, "Design of Narrow Discrete Distances of Dual-/Triple-Band Terahertz Metamaterial Absorbers," Nanoscale Res. Lett. **14**(1), 64 (2019).
23. Z. Song, K. Wang, J. Li, and Q. H. Liu, "Broadband tunable terahertz absorber based on vanadium dioxide metamaterials," Opt. Express **26**(6), 7148–7154 (2018).
24. W. Meng, J. Lv, L. Que, Y. Zhou, and Y. Jiang, "A multi-band terahertz metamaterial absorber with novel structure," *9th International Symposium on Advanced Optical Manufacturing and Testing Technologies*, Chengdu, (China, 2018).

Optics EXPRESS

25. Y. Cheng, H. Zou, J. Yang, X. Mao, and R. Gong, "Dual and broadband terahertz metamaterial absorber based on a compact resonator structure," Opt. Mater. Express **8**(10), 3104–3114 (2018).
26. H. Xiong, Y.-B. Wu, J. Dong, M.-C. Tang, Y.-N. Jiang, and X.-P. Zeng, "Ultra-thin and broadband tunable metamaterial graphene absorber," Opt. Express **26**(2), 1681–1688 (2018).
27. B. X. Wang, X. Zhai, G. Z. Wang, W. Q. Huang, and L. L. Wang, "Design of a Four-Band and Polarization-Insensitive Terahertz Metamaterial Absorber," IEEE Photonics J. **7**(1), 4600108 (2015).
28. W. Pan, X. Yu, J. Zhang, and W. Zeng, "A novel design of broadband terahertz metamaterial absorber based on nested circle rings," IEEE Photonics Technol. Lett. **28**(21), 2335–2338 (2016).
29. K. Bi, D. Yang, J. Chen, Q. Wang, H. Wu, C. Lan, and Y. Yang, "Experimental demonstration of ultra-large-scale terahertz all-dielectric metamaterials," Photonics Res. **7**(4), 457–463 (2019).
30. M. Watanabe, S. Kuroda, H. Yamawaki, and M. Shiwa, "Terahertz dielectric properties of plasma-sprayed thermal-barrier coatings," Surf. Coat. Technol. **205**(19), 4620–4626 (2011).
31. D. Zhang, Y. Yang, Z. Geng, B. Cui, and R. Zhao, "A High-Selectivity THz Filter Based on a Flexible Polyimide Film," IEEE Trans. THz Sci. Technol. **8**(6), 719–724 (2018).
32. H. T. Chen, "Interference theory of metamaterial perfect absorbers," Opt. Express **20**(7), 7165–7172 (2012).
33. T. Wanghuang, W. Chen, Y. Huang, and G. Wen, "Analysis of metamaterial absorber in normal and oblique incidence by using interference theory," AIP Adv. **3**(10), 102118 (2013).
34. Y. Cheng, H. Zou, J. Yang, X. Mao, and R. Gong, "Dual and broadband terahertz metamaterial absorber based on a compact resonator structure," Opt. Mater. Express. **8**(10), 3104–3114 (2018).